Waves in the chromosphere: observations[*]

R.J. Rutten

Sterrekundig Instituut, Utrecht University
Institute for Theoretical Astrophysics, Oslo University

January 23, 2003

Abstract

I review the literature on observational aspects of waves in the solar chromosphere in the first part of this contribution. High-frequency waves are invoked to build elaborate cool-star chromosphere heating theories but have not been detected decisively so far, neither as magnetic modes in network elements nor as acoustic modes in below-the-canopy internetwork regions. Three-minute upward-propagating acoustic shocks are thoroughly established through numerical simulation as the cause of intermittent bright internetwork grains, but their pistoning and their role in the low-chromosphere energy budget remain in debate. Three-minute wave interaction with magnetic canopies is a newer interest, presently progressing through numerical simulation. Three-minute umbral flashes and running penumbral waves seem a similar acoustic-shock phenomenon awaiting numerical simulation. The low-frequency network Doppler modulation remains enigmatic.

In the second part, I address low-frequency ultraviolet brightness variations of the internetwork chromosphere in more detail. They contribute about half of the internetwork brightness modulation and presumably figure in cool-star basal flux. They appear to be a mixture of inverse-contrast granular overshoot at small scales and gravity-wave interference at mesogranular scales. I present TRACE evidence for the latter interpretation, and speculate that the low-frequency brightness minima map canopy heights.

1 Introduction

Waves in the solar chromosphere may be divided in many different ways: high versus low chromosphere, below the canopy versus above the canopy, network versus internetwork, acoustic versus magnetic versus gravity mode, linear versus shocks, quiet versus active region, standing versus propagating versus evanescent, global versus local, short-period versus three-minute versus five-minute versus long-period, longitudinal versus transverse versus torsional. And, in particular, whether they heat appreciably or negligibly. The latter issue is the most frequently quoted motivation for chromospheric wave studies and for their claims to fame, but it seems to me that identifying the nature of the observed modulations and the underlying processes and interactions should come first – and, personally, I regard the physics as more interesting than the eventually resulting overall energy budget, a mere summation at the very end with the answer already known as balancing photon losses.

---

[*]Appeared in the proceedings of a NATO Advanced Research Workshop held at Budapest in 2002 edited by Erdélyi et al. (2003) but not entered or even listed on ADS through laxness of the publisher and editors. Submitted to arXiv Astro-ph on December 6, 2010 to remedy this neglect and to demonstrate my newest latex trick: in on-screen reading, clicking on the year in each citation opens the corresponding ADS abstract page in your browser. Explanation: `http://www.astro.uu.nl/~rutten`.

2   Overview

In this section I briefly review the literature[1] using the above splits as guideline.

Chromosphere. Even this term is non-trivial. In the standard one-dimensional modeling of Vernazza, Avrett & Loeser (1973, 1976, 1981) and Fontenla et al. (1993), it denotes the plane-parallel layers between the temperature minimum and the onset of the coronal temperature rise. Within this definition, UV continua shortward of 1600 Å come from the chromosphere (VALIII Fig. 36 in Vernazza et al. 1981), and strong optical lines are also chromospheric – but not always. For example, the Na I D lines reach $\tau = 1$ above the VALIII temperature minimum, but they are photospheric in their intensity response and do not map the chromospheric temperature rise in their VALIII emergent profiles (Bruls et al. 1992). Even Ca II K filtergrams primarily sample the upper photosphere since the intensity-encoding thermal creation (rather than the velocity-encoding last scattering) of most of the observed photons takes place well below the VALIII minimum. In addition, the existence of a ubiquitous temperature starting at $h = 500$ km has been put into doubt, first by Ayres' CO modeling (e.g., Ayres & Testerman 1981; Ayres 1981; Ayres et al. 1986; Ayres & Wiedemann 1989; Ayres & Brault 1990; Ayres & Rabin 1996) and subsequently by the Carlsson–Stein acoustic shock modeling (see below).

Hence, I prefer to define "chromosphere" – harking back to its eclipse origin = the purple color of $H\alpha$ plus $H\beta$ off-limb emission – as the solar regime characteristically sampled by Balmer lines as a complex mass of fibrils, and taking the latter to represent (incomplete!) mappings of magnetic canopies[2].

Canopies. The concept comes from Giovanelli (1980), Jones & Giovanelli (1982), Giovanelli & Jones (1982) and is portrayed in older models and recent simulations (e.g., Bünte et al. 1993; Rosenthal et al. 2002; Bogdan et al. 2002) as smoothly upward spreading field hovering dome-like over essentially field-free internetwork. This is a simplification. If we define the chromosphere to start at canopy height (the height where the plasma beta drops through unity), its lower boundary will actually be a very warped surface, offset by dynamical flows and with large topological variations defined by the small-scale and large-scale field strength and connectivity, as partially delineated by $H\alpha$ as short local and long distant fibril connections (cf. Schrijver & Title 2002).

High versus low chromosphere. This distinction now means well above and just above the canopy, respectively. Most of the references in this review pertain to the low chromosphere or even the upper photosphere (say $h = 400 - 800$ km). Higher up, most of the recent wave literature employs CDS and SUMER spectrometry to discuss to what height the internetwork three-minute oscillations penetrate (e.g., Steffens et al. 1997; Carlsson et al. 1997; Judge et al. 1997; Doyle et al. 1998; Curdt & Heinzel 1998; Gouttebroze et al. 1999; Doyle et al. 1999; Wikstøl et al. 2000; Judge et al. 2001; McIntosh & Judge 2001). Such penetration is likely to vary strongly with the actual field geometry. Oscillation analyses in tandem with moss and coronal loop diagnostics are yet scarce (but see Ineke de Moortel's contribution in this volume).

Theoretical insight comes from beautiful Oslo simulations (Rosenthal et al. 2002; cf. Bogdan et al. 2002). I wonder whether such simulations for different stellar parameters may, at long last, explain the Wilson-Bappu relation between stellar luminosity and Ca II H & K peak width (Wilson & Vainu Bappu 1957). It must describe fluxtube atmosphere properties, rather than non-magnetic

---

[1]Note added December 5, 2010: All ADS abstracts for almost all solar physicists cited in this paper are collected at `http://www.astro.uu.nl/~rutten/solar_abstracts`.

[2]The definition implies that chromospheric studies must include $H\alpha$ even though its formation is singularly awkward through mixing thickness and thinness with NLTE opacity and source function sensitivities including Zanstra-like ionisation-plus-recombination photon conversions. An unpleasant but inescapable conclusion to one prefering clean lines such as Ca II H & K. Quantitative $H\alpha$ mapping requires considerable work on reliable $H\alpha$ interpretation, comparable to the ongoing efforts in Stokes profile inversion.

atmospheric stratifications (e.g., Ayres 1979; Kneer 1983), since the emission peaks come from the magnetic component.

Network versus internetwork. This division is also overly simplistic. The verdict on internetwork fields isn't yet in, but they exist undoubtedly at some level of field strength and scale of spatial organization. Ca II K and TRACE UV image sequences show extended zones of enhanced brightness (with respect to the darkest "cell centers") as aureoles around network (cf. Fig. 5). Acoustic maps show similar three-minute power aureoles when sampling power below the canopy and power shadows above it (e.g., Braun et al. 1992; Brown et al. 1992; Toner & Labonte 1993; Hindman & Brown 1998; Lindsey & Braun 1999; Braun & Lindsey 1999; Thomas & Stanchfield 2000; McIntosh et al. 2001; Judge et al. 2001; McIntosh & Judge 2001; Krijger et al. 2001).

In addition, Ca II K and TRACE UV image sequences also show evidence of "magnetic flashers", presumably isolated fluxtubes on their way to or from the network concentrations (Brandt et al., 1992, 1994; Nindos & Zirin 1998; Lites et al. 1999; Krijger et al. 2001). Their isolation may be helpful in trying to identify chromospheric tube modes excited by convective buffeting without amplitude loss from phase mixing over multiple fluxtubes.

Acoustic versus magnetic versus gravity modes. Or mixtures, of course. *Magnetic modes* are often invoked to convey energy from photospheric buffeting up along network fluxtubes (e.g., Hasan & Kalkofen 1999; Hasan et al. 2000) but have not been convincingly diagnosed yet, except negatively as suppression of acoustic wave power by conversion at canopies (McIntosh et al. 2001; McIntosh & Judge 2001; Rosenthal et al. 2002).

Internal gravity waves should be "copiously excited" in granular overshoot according to theory (e.g., Whitaker 1963; Lighthill in Thomas 1967; Stein 1967; Schmieder 1977; Mihalas & Toomre 1981, 1982), but they are difficult to detect, being small-scale and propagating slantedly. The observational evidence is mostly indirect (Frazier 1968; Schmieder 1976; Cram 1978; Brown & Harrison 1980; Durrant & Nesis 1981; Staiger et al. 1984; Staiger 1987; Deubner & Fleck 1989; Bonet et al. 1991; Komm et al. 1991), with the clearest demonstration coming from wavenumber- and frequency-resolved (k_h, f) phase-difference spectra (Kneer & von Uexküll 1993; Straus & Bonaccini 1997; Krijger et al. 2001). Whether they affect upper-photosphere or low-chromosphere energy balances is not known. See also Section 3 below.

Linear versus shock behavior. At least in the case of the three-minute oscillation, protests against large non-linearity (Deubner 1991) were silenced by the successful reproduction of so-called Ca II H_{2V} grain behavior in the celebrated simulations of Carlsson and Stein (1994, 1996, 1997; Stein & Carlsson 1997) of the spectral time sequences of Lites et al. (1993). The Carlsson-Stein reproduction of complex spectral Ca II H core evolution patterns identified the three-minute oscillation beyond doubt with upward propagating acoustic shock trains, as proposed earlier by Athay (1970), Cram (1972), Liu & Skumanich (1974), Mein et al. (1987), Leibacher et al. (1982), Rutten & Uitenbroek (1991b, 1991a) and Rammacher & Ulmschneider (1992). However, the nature of the photospheric pistoning remains in debate (Nindos & Zirin 1998; Lites et al. 1999; Worden et al. 1999; Sivaraman et al. 2000; Skartlien et al. 2000; Hoekzema et al. 2002, as does the role or absence of a role in chromospheric heating (Carlsson & Stein 1995; Theurer et al. 1997a; Kalkofen et al. 1999; Kalkofen 2001). See also Section 3 below.

Active region oscillations. A direct active-region counterpart to the quiet-sun three-minute oscillation consists of the three-minute oscillations producing *umbral flashes* (Beckers & Tallant 1969). They show even more outspoken nonlinear character (e.g., Thomas et al. 1984; Lites 1986), and are most likely similar nearly-acoustic shock trains running up along the radial fields above umbrae as suggested by Lites

(1992, 1994) Some are observed to penetrate up into coronal loops in UV and EUV data (e.g., Brynildsen et al., 1999, 2002; Maltby et al., 1999, 2001; Schrijver et al. 1999) and in microwave observations (Gelfreikh et al. 1999; Shibasaki 2001; Nindos et al. 2002).

Similarly, *running penumbral waves* (Zirin & Stein 1972; Alissandrakis et al. 1992; Brisken & Zirin 1997; Christopoulou et al., 2000, 2000, 2001, 2002) may harbor complex wave reflection and mode conversion as postulated by Bogdan et al. 2002 from comparison to thinner fluxtubes, but recent high-resolution data from three solar telescopes on La Palma suggest strongly that running penumbral waves and umbral flashes are both upward-propagating acoustic shock trains, seen differently through difference in field alignment with the line of sight and with the apparent horizontal spreading primarily a mapping of the field geometry (Rouppe van der Voort et al. 2003). Oslo simulations as those of Carlsson & Stein (1997) are needed for decisive diagnosis, including "calibration" of the polarimetric umbral-flash inversions of Socas-Navarro et al. (2001) through less indirect forward modeling.

The existence and nature of oscillations in the sunspot magnetic field itself remain contested (e.g., Lites et al. 1998; Balthasar 1999; Staude 2002: Kupke et al. 2000), with Settele et al. (2002) warning against instrumental crosstalk and initial results from infrared spectropolarimetry indicating that opacity variations are an alternative explanation (cf. Collados 2002; Khomenko et al. 2003). Georgakilas et al. (2002) found indications from TRACE data that running penumbral waves even spread into sunspot moats.

Chromospheric oscillations above plage have not received much attention in the literature, but Rita Ryutova's presentation of beautiful TRACE 171 Å time slices from Richard Shine show interesting braiding with shorter braid period at larger magnetic filling factor (see her contribution in these proceedings).

Standing versus propagation. This issue is also debated in the three-minute oscillation literature (Deubner et al., 1992, 1996; Steffens et al. 1995; Hofmann et al. 1996; Deubner 1998). with simulations showing that at least some of the observed standing-wave behavior comes from reflections off the grain-forming shocks themselves and off canopies (Carlsson & Stein 1999; Rosenthal et al. 2002).

Another standing versus propagation issue concerns the nature of the so-called pseudo-ridges above the cutoff frequency in (k_h, f) diagrams, also a global-versus-local issue. Kumar (1994) described them as interference between directly emitted and once-bounced outgoing waves (that propagate up rather than being evanescent), using "interference" as a misleading mathematical term describing low-l Fourier decomposition. Physically there is no actual wave interference, but simply power addition in (k_h, f) diagrams at those (k_h, f) locations that sample one-bounce horizontal spatial wavelengths at the corresponding temporal frequency, just another expression of the single-bounce three-minute power ridge in time-distance plots (Duvall et al. 1993) and exhibiting the Duvall dispersion law (Duvall 1982; Eq. 2.14 of Deubner & Gough 1984). Below the cutoff frequency, the acoustic ridges describe evanescent p-modes, with small phase delays compared to the photosphere governed by non-adiabaticity (Krijger et al. 2001).

Short-period versus three-minute versus five-minute versus low-frequency modulation. These terms are all often misnomers. By *short-period waves* one simply implies those that might after all heat the chromosphere, with Peter Ulmschneider with coworkers as tenacious champion. After giving up on five-minute heating when the p-modes were identified and on three-minute heating when the Carlsson–Stein simulation refuted a low-lying chromospheric temperature rise, his quest turned to higher-frequency components not present in the Carlsson-Stein piston (e.g., Sutmann & Ulmschneider 1995; Theurer et al., 1997a, 1997b; Kalkofen et al. 1999) with obvious stellar overtones (Ulmschneider et al. 1996, Cuntz et al. 1999), and more recently to adding longitudinal, transverse and torsional tube waves (Ulmschneider et al., 2001b, 2001a; Musielak and Ulmschneider, 2002, 2002a, 2002b) as well as detailed theoretical prediction of the mix of acoustic and tube waves that should explain observed cool-star chromospheric photon losses with the magnetic filling factor as activity scaling parameter (Fawzy et al., 2002a, 2002c, 2002b).

Heating by 10–100 mHz waves, outside and inside fluxtubes, is probable; the question is to

what extent. Observationally, they are hard to see since they require fast cadence and high angular resolution and suffer response function loss by vertical wavelengths fitting in contribution functions (e.g., Schmieder & Mein 1980; Durrant 1980) and through large sensitivity to seeing noise (e.g., Endler & Deubner 1983; Deubner et al. 1984; Lites et al. 1994). Indeed, the trials to detect high-frequency waves remain inconclusive (e.g., Deubner 1976; Lites & Chipman 1979; Mein & Schmieder 1981; Deubner & Fleck 1990; Krijger et al. 2001).

The chromospheric *three-minute* and *five-minute* oscillations are discussed above. The names imply broad-band frequency domains, not specific periodicities but just a shift in dominance from five-minute to three-minute periodicity when rising from the photosphere up to the chromosphere (in the internetwork at least). It is therefore also wrong to call them chromospheric and photospheric, respectively. The original Leighton-Simon-Noyes era diagram in Noyes (1967), reprinted in Rutten (1995, 2001) clearly demonstrates the gradual change.

Finally, *low-frequency oscillations* is a misnomer when the observed modulation is not oscillatory. This may hold for the observed low-frequency Dopplershift power of chomospheric network which may result from convective fluxtube buffeting (cf. Kneer and von Uexküll 1985, 1986; von Uexküll et al. 1989; Lites et al. 1993; Hasan et al. 2000), and also for low-frequency low-chromosphere internetwork oscillations if granular overshoot rather than internal gravity waves dominates the observed low-frequency power.

3 Low-frequency internetwork background modulation

I devote the remainder of this contribution to the topic on which I concentrated in my oral presentation at the meeting: the nature of the low-frequency background in low-chromosphere ("upper photosphere" in the under-the-canopy definition) image sequences. I have long been puzzled by the mesh-like background pattern underlying K_{2V} grains in Ca II K image sequences (cf. Lites et al. 1999). The upshot is that I believe the answer to be a mixture of granular overshoot plus gravity-wave interference at slightly larger scales. I advocate this interpretation with selected results from TRACE data analyzed by J.M. Krijger in his PhD thesis (Krijger 2002). The diagrams in this section also illustrate various points made above[3].

The observation and reduction details are given in Krijger et al. (2001). The displays below come from the very quiet-sun data taken on October 14, 1998, when TRACE registered image sequences in its 1700, 1600 and 1550 Å ultraviolet passbands and also in white light. The combination permits comparison of photospheric brightness patterns to the co-spatial and co-temporal ultraviolet ones. Such comparisons used to be made with groundbased telescopes combining Ca II K and continuum image registration (e.g., Hoekzema et al., 1998, 1998, 2002) but TRACE furnishes better quality thanks to the absence of seeing in space[4].

Space-time representations. Figure 1 defines the topic. It compares the white-light low-photosphere scene with the co-spatial and co-temporal 1700 Å high-photosphere scene in the upper panels. The lower panels compare evolutionary characteristics between the two regimes. The displays sample only very small parts of the full white-light and 1700 Å data cubes[5].

The difference between dark internetwork and bright network is obvious in the ultraviolet image (second column). The network grains stand out even though their brightness is cut in half by the display scaling. TRACE's resolution (1 arcsec) is insufficient to resolve the corresponding white-light "network bright points" (magnetic elements) residing within the underlying intergranular lanes.

---

[3]Note added on December 5, 2010: part of this work was published in Rutten & Krijger (2003) but not all diagrams and ideas given here survived the referee.

[4]But the tide turns, now that speckle reconstruction, phase-diverse restoration and adaptive optics also do away with (most of) the seeing, permitting higher angular resolution than TRACE's 1 arcsec. Much sharper images now result e.g., from our Dutch Open Telescope which is presently being equipped with multi-wavelength tomography capability (`http://dot.astro.uu.nl`).

[5]These cutouts are small in order to obtain sufficient magnification. They represent a very limited rendering of the full data cubes. A better view of the dynamical ultraviolet scene is gained by inspecting the TRACE movies available at `http://www.astro.uu.nl/~rutten/trace1`.
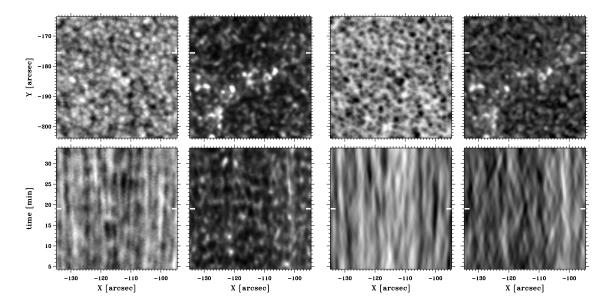
Figure 1: TRACE image and time-slice samples. First column: white-light intensity. Second column: co-temporal and co-spatial 1700 Å intensity. The images in the upper row are small cut-outs of the full 256×256 arcsec² field shown in Fig. 5. The time of observation is halfway the time slices in the lower row, as indicated by white markers. The slices show the temporal intensity evolution during 30 min of observation, for a horizontal cut through an internetwork area indicated by the white markers in the upper panels. It passes through weak network at the right. In the first two columns the greyscale is linear for all four panels, but it has been clipped at half the actual maximum for the 1700 Å image to enhance internetwork. Third and fourth column: the same, but low-pass filtered (subsonic horizontal propagation only). Third column: white-light brightness on a sign-reversed greyscale. Fourth column: logarithm of the 1700 Å brughtness temperature.

The white-light time slice in the lower-left panel displays primarily granular evolution, with some larger-scale five-minute p-mode modulation. The ultraviolet time slice shows the dynamical behavior characteristic of internetwork in the form of ubiquitous short-lived three-minute oscillation sequences. The brightest phases are called internetwork grains. The weak network grain near $X = -100$ arcsec stands out by its relative longevity. Note that the cut selection favours internetwork; stronger network grains produce much brighter vertical streaks.

The two righthand columns show the same data after Fourier filtering and with modified greyscaling. In the third column (white light) low-pass "subsonic' filtering, i.e., applying a 3D Fourier "cone" filter to the transformed data cube which passes all signals with apparent horizontal speed below the sound speed, has removed the photospheric five-minute oscillation so that only the granular evolution patterns remain. In addition, the greyscale is sign-reversed to simulate "reversed granulation" with reversed contrast. The resulting mesh pattern in the reversed image illustrates the topological difference between granules and intergranular lanes. The corresponding time slice shows intergranular lanes as rather long-lived bright streaks.

In the fourth column (1700 Å) the low-pass filtering has removed the chromospheric three-minute oscillation and therefore emphasizes the slower background evolution. The background streaks are relatively short and show larger horizontal displacements (tilts) than the intergranular streaks. At this resolution, there is no obvious correspondence between the reversed low-frequency granular evolution pattern in the third slice and the low-frequency internetwork background modulation pattern in the fourth slice.
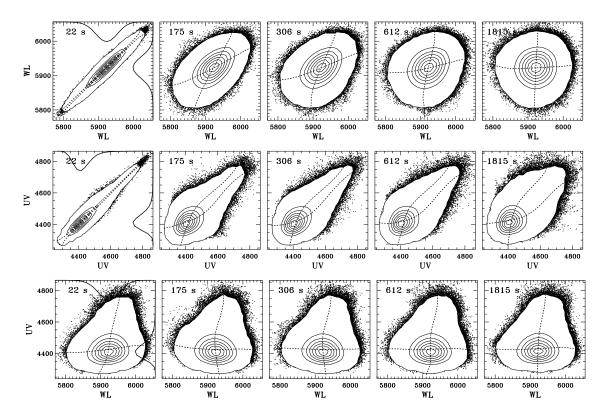
Figure 2: Strous-format scatter diagrams. The crowded central parts are plotted as sample density contours to avoid plot saturation. First row: time-delayed white-light brightness temperature in K WL(t + Δt) against WL(t). Second row: time-delayed 1700Å brightness temperature UV(t + Δt) against UV(t). Third row: UV(t + Δt) against WL(t). The time delays Δt are specified in each panel and increase from left to right. The solid curves in the first panels show the occurrence distributions of the quantities plotted along x and y on inverted normalized scales. The dashed curves show the first moments of the sample density along horizontal and vertical cuts through the contours.

Time-delay scatter representations.   Figures 2–3 are pixel-by-pixel dual-image correlation plots in an informative format initiated by Strous (1994). Each plot is measured from a $256 \times 256\,\text{px}^2$ TRACE subfield after removal of Fourier taper edges, image conversion into brightness temperature, and $1.5 \times 1.5\,\text{arcsec}^2$ boxcar smoothing to suppress noise.

For each pixel in the subfield, i.e., each solar location, the brightness temperature at one moment in the one type of image (say white light = WL) is taken as x quantity plotted horizontally, its value at another (later) moment in the other type of image (say 1700 Å = UV) as y quantity plotted vertically. The pair defines one point in a scatter plot. Such pairwise comparisons are made for all pixels (solar locations) in the whole subfield or in some selective part of it, and repeated for 50 consecutive image pairs to gain high significance (millions of spatio-temporal samples). Plot saturation (total blackness) is avoided by plotting sample density contours instead of the individual pixel-by-pixel samples.

The WL–WL comparison in the first row of Fig. 2 illustrates the format. Brightness distribution curves are added in the first panel. They are virtually the same for the other panels and also along x and y in this auto-correlation sequence. For 100% correlation all samples and both first-moment (center of gravity) curves lie along the forward diagonal. For 100% anticorrelation they lie along the backward diagonal. At the absence of any correlation the first-moment curves become perpendicular, parallel to the axes, and
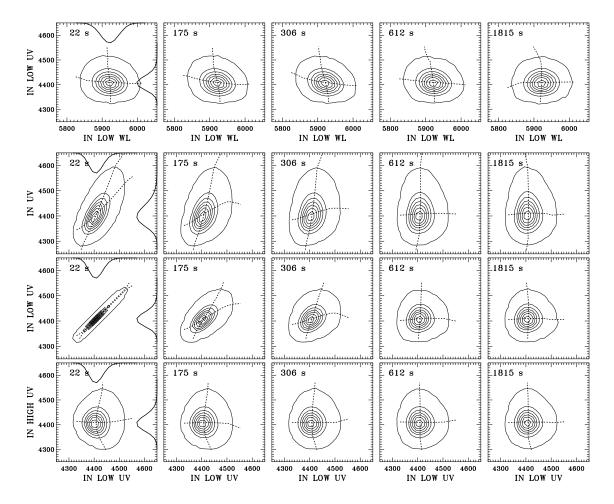
Figure 3: Time-delay scatter diagrams as in Fig. 2 but for internetwork (IN) only. First row: time-delayed low-pass filtered 1700 Å brightness temperature UV(t + Δt) against low-pass filtered white-light brightness temperature WL(t). Second row: unfiltered UV against low-pass UV. Third row: low-pass UV against low-pass UV. Fourth row: high-pass UV against low-pass UV, with the mean UV internetwork value (T_b = 4418 K) added to the high-pass UV modulation for y-axis compatibility.

the contours become circular if the distribution function is symmetric. From left to right the panels have increasing time delay between the sampling of each type of image per solar location. The initial panel for Δt = 22 s shows very high pattern correlation because the granulation has not changed much during this brief interval. The final panel for Δt = 30 min shows absence of pattern correlation in the form of non-aligned first-moment curves and a nearly round bull's-eye contour pattern. The sequence illustrates that granulation largely loses its pattern identity over ten minutes, completely in half an hour.

The UV–UV autocorrelation sequence in the second row illustrates the two-component dichotomy between chromospheric network and internetwork. The bright upward distribution tail made up by network grains persists over long delays, whereas the darker internetwork (lower-left contour mountain) shows faster pattern change.

The UV–WL cross-correlation sequence in the bottom row of Fig. 2 shows some persistent bright-bright correlation due to network, slight anticorrelation for low WL at Δt = 3 min, and subsequent lack of persistent correlation at low UV brightness.

In Fig. 3 the ultraviolet signal is decomposed in constituents by using selective data subsets for similar scatter diagrams. All four rows are limited to internetwork (IN) areas only. Fourier cone filtering as in Fig. 1 is applied to show low-pass signals (apparent horizontal propagation below 6 km s^{-1}) or high-pass signals (above 7 km s^{-1}) only, selecting acoustic and non-acoustic modulation. The corresponding reduction in sampling statistics is offset by extending the pixel-by-pixel sampling to 120 consecutive image pairs per comparison (in all scatter plots the outer contour lies at 100 samples per bin with 25 bins per axis). The outer scatter clouds are now excluded to reduce the plot file size.

The first row of Fig. 3 plots low-pass UV against low-pass WL. There is a slight but persistent anticorrelation over time delay $\Delta t = 2 - 6$ min. I attribute it to reversed granulation and expect it to become stronger in higher-resolution data that resolve granulation better than TRACE does. The slightness of the correlation shows that at the somewhat larger meso-scales imaged properly by TRACE, something else is present that does not obey point-to-point correlation or counter-correlation with the underlying photosphere at any time delay.

The remaining three rows decompose the UV signal in high-frequency and low-frequency components, as contributed by the latter (low-pass UV as x-axis quantity). The second row plots total UV against low-pass UV in internetwork. The high initial correlation, with a roughly 2:1 slope, shows that peaks in internetwork UV brightness, i.e., internetwork grains, occur preferentially when also the slow-changing internetwork background is bright. This strong correlation is conform the finding of Cram & Damé (1983) that bright Ca II H$_{2V}$ grains are invariably part of a larger-scale modulation pattern. The same happens in the ultraviolet continua. Thus, the slowly evolving background pattern and the three-minute oscillation combine constructively to produce bright internetwork grains, each contributing about half of the excess brightness temperature. This makes the background a much more important grain co-localizer[6] than e.g., acoustic events (cf. Hoekzema et al. 2002).

The next row shows a low-pass internetwork-only UV autocorrelation sequence. It illustrates the five-minute lifetime of the low-frequency pattern at a given spatial position. Horizontal propagation – seen as tilts in the low-pass UV time slice in the final panel of Fig. 1 when having an x component – causes loss of scatter correlation when the travel exceeds the 1.5 arcsec boxcar smoothing.

The final row correlates high-pass UV with low-pass UV in internetwork. The curved shape of the vertical moment curves indicates that large three-minute excursions, both to high and to low UV brightness temperature with respect to the mean after removal of all slow variations, tend partially toward correlation with large UV background amplitude. This implies that the three-minute oscillation partially has modulatory character, gaining larger oscillation amplitude at larger background amplitude. The effect is not large. In addition, the contours have slightly asymmetric shape indicating non-linearity in wave behavior. When plotted as intensity, the scatter clouds stretch much further upwards due to the non-linear Planck function response in the ultraviolet. The conversion to brightness temperature circularizes the contours considerably.

The conclusions from Figs. 2–3 are, first, that the slowly-evolving internetwork ultraviolet background contributes about half of internetwork grain brightness excesses, in addition to the acoustic modulation modeled by Carlsson & Stein, and, second, that at TRACE's meso-granular resolution this background seems to be something else than reversed granulation.

Fourier representations. Figure 4 compares the same TRACE data in terms of (k_h, f) Fourier phase differences, at left between 1700 and 1600 Å brightness, at right between white-light and 1700 Å brightness. The acoustic oscillations (ridges and pseudo-ridges) in a similar diagram from the May 12, 1998 TRACE data are discussed in Sect. 4.4 of Krijger et al. (2001); the emphasis here lies on the low-frequency domain. Note that the October 14, 1998 TRACE data contain only very weak network (cf. Fig. 5) so that these (k_h, f) diagrams are dominated by internetwork behavior.

---

[6]The low-frequency background was not part of the Carlsson-Stein simulation. The corresponding Dopplershifts have less power than the brightness modulation and were not part of the Carlsson-Stein iron-blend piston because they were removed in spectrograph drift correction by Lites et al. (1993).
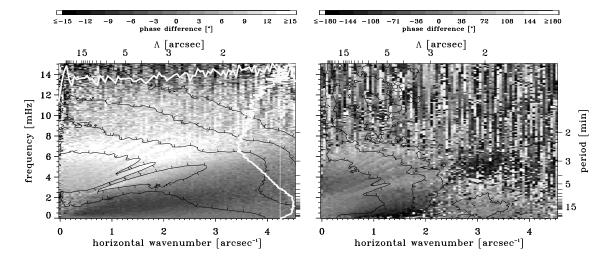
Figure 4: Two-dimensional Fourier spectra from TRACE. Lefthand graph: $\Delta\phi(1700-1600)$ intensity phase difference. Axes: horizontal wavenumber k_h and temporal frequency f. The corresponding wavelengths and periodicities are specified along the top and righthand side. Greyscale: phase difference coding specified in the bar above the graph. The white curves along the sides are the temporal and spatial means, on linear scales in arbitrary units. The contours specify $1700-1600$Å coherence at values $C = 0.4, 0.6, 0.8$ and 0.95, with the ticks directed to lower values. Righthand graph: similar $\Delta\phi(WL-1700)$ phase difference spectrum between white light intensity and 1700Å intensity. The contours specify coherence levels $C = 0.1, 0.2$ and 0.5. Thijs Krijger production.

The lefthand graph shows a prominent wedge-shaped signature of negative propagation over a large k_h range. It has high coherence between 1700 and 1600 Å modulation. The wedge location, its Lamb-line delimitation, and its negative values all suggest atmospheric gravity waves as cause. The large coherence implies that these waves dominate the low-frequency internetwork background in the ultraviolet at meso-scale wavelengths.

The righthand (k_h, f) diagram is very noisy but again shows a low-f low-k wedge of negative phase for $k_h < 2$ arcsec^{-1}, i.e., at mesogranular scales. It reaches much larger $\Delta\phi$ values due to the much larger span in formation height and it has much smaller coherence, but it is qualitatively similar. At larger k_h the low-f phase differences flips from large negative to large positive values at about $k_h = 2.5$ arcsec^{-1}, attributed to wraparound in the $\Delta\phi = [-180, +180]$ deg evaluation. This makes the positive blob around $k_h = 3$ arcsec^{-1} (outlined by a $C = 0.1$ coherence contour) a continuation of the negative dark wedge, presumably marking reverse granulation. The slight counter-correlation signature in the top row of Fig. 3 is therefore indeed caused at granular scales. This high-k contribution is likely to become better defined at higher angular resolution than TRACE. The mesoscale negative-phase blob in the righthand (k_h, f) diagram describes the non-correlated other agent, which I attribute to internal gravity waves.

Discussion. In summary, it seems that the slowly-evolving background mesh pattern in the internetwork parts of chromospheric image sequences is made up of reversed granulation and internal gravity waves at slightly larger scales.

Numerical simulation may address this interpretation beyond speculation. Obviously, this should be feasible with realistic numerical simulations of the solar granulation such as those of Stein & Nordlund (1998) when equipped with sufficient atmosphere as in Skartlien et al. (2000). They should reproduce both granular overshoot and gravity-wave emission. The two phenomena are akin but not identical, since overshoot is

a local phenomenon whereas gravity waves spread away from their source, interfere, and break at relatively large height (cf. Mihalas & Toomre 1981).

Basal flux.   The demonstration in Fig. 3 that roughly half of the brightness excess in internetwork grains is contributed by the low-frequency variation applies likewise to Ca II K$_{2V}$ grains and the accompanying Ca II K line-core and inner-wing brightness modulation. Since the solar internetwork scene observed in Ca II K is dominated by the superposition of these acoustic and low-frequency variations, the corollary is that part of the basal flux observed from non-active cool stars Schrijver 1995, and references therein, is attributable to similar combination of acoustic and low-frequency phenomena including gravity waves – not just acoustics alone.

Internetwork fields.   As noted in Section 2 the debate on the pistoning of internetwork grains continues. It includes pro-and-contra claims on internetwork fields as grain localiser. Advocates pro may argue that the 50% grain co-localization by the low-frequency chromospheric background pattern seen in Fig. 3 results from weak fields that are swept into intergranular lanes without reaching the magnetic flux of network elements, as suggested observationally by Lin & Rimmele (1999) and theoretically by the magnetoconvection simulations of Emonet & Cattaneo (2001), on the assumption that such small concentrations share the network habits of being bright in the chromosphere and displaying low-frequency variations there.

I rather doubt this alternative explanation because of the ubiquity and regularity of the background emission, the low counter-correlation to intergranular lanes for the spatial "meso"-scales producing the negative-phase blob in Fig. 4, and the issue how intrinsically weak fields would influence the thermodynamics of the low chromosphere. The inverse-amplitude mapping in Fig. 5 discussed below suggests rather the reverse to me, namely that larger low-frequency modulation amplitude implies weaker magnetism.

Nevertheless, internetwork magnetism cannot be rejected as a chromospheric brightness producer. I wonder whether it may play a role in the generation of small-scale reversed granulation, in the form of kilogauss fluxtubes that are too thin to be magnetographically observable so far. One reason for such wondering is the wide extent of relatively bright areas surrounding chromospheric network the "intermediate" pixel class of Krijger et al. 2001, suggesting searches for relations between the occurrence of reversed granulation and magnetic flux density in high-resolution large-sensitivity magnetograms.

Inverse canopy mapping.   Finally, Fig. 5 serves to illustrate a speculation bringing me back to the first item in my review above: the definition of the canopy as lower chromosphere boundary. It shows a one-hour temporal average of the 1700 Å brightness over the full TRACE field, with inverted (1/value) greyscale. The inversion de-emphasizes network grains by making them dark. The hour-long averaging reduces the three-minute component; remaining enhancements from internetwork grain nonlinearity (non-sinusoidal spikes) also become dark. Thus, the brightest features in this display mark locations where the low-frequency background modulation reaches its deepest minima without contamination by other phenomena.

Figure 5 shows a grainy pattern. The brightest grains mark preponderance of extreme low-frequency minima. In reversed-granulation terms, these should correspond to long-lived or repetitive bright granules surviving a full hour of temporal averaging. Their distribution over the many network cells covered by Fig. 5 clearly shows preference for the internetwork centers, with striking avoidance of the cell boundaries.

My speculation is that such preferential occurrence of low-frequency extrema marks locations where the magnetic canopy reaches larger height than elsewhere. In the gravity-wave interpretation, amplitude reduction may occur where the field becomes strong enough to convert gravity waves into other modes or to reflect them. The areas containing the brightest inverse grains in Fig. 5 would then have the highest canopy, giving the waves more room to increase their amplitude – I suspect up to wave-breaking height.

A reverse speculation by our meeting's co-director R. Erdelyi is that magnetic resonant absorption enhances specific wave modes at the canopy height and that large apparent amplitude may mark such resonance (cf. Cadez et al. 1997; Pintér et al. 2001).
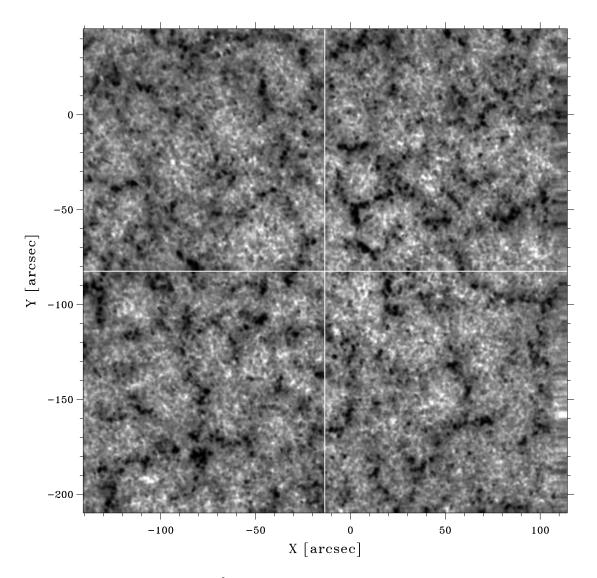
Figure 5: Temporally-averaged 1700 Å brightness on an inverted greyscale. The white lines mark division into smaller quadrants for processing. The yet smaller subfield of Fig. 1 is near the lower-left corner. The horizontal striping near the right edge results from solar rotation correction.

4   Conclusion

Both the review in Section 2 and the ultraviolet background analysis in Section 3 are observationally oriented. However, the major advance in chromospheric wave research in the past years is, in my view, the advent of realistic detailed simulations, in particular radiation (magneto-)hydrodynamic simulations casting Scandinavians and Robert F. Stein as coauthors. Of course, I allude to the Carlsson & Stein (1997) acoustic propagation simulation, the Skartlien et al. (2000) acoustic excitation simulation, and the Rosenthal et al. (2002) shaken-fluxtube and canopy-interaction MHD simulation. An

important strength of these simulations is that they are unusually close to observations, firstly in aiming to reproduce particular observed phenomena rather than prove grand presupposed concepts, secondly in the use of elaborate observation-like diagnostics to analyse simulation physics rather than just showing overall results.

The issues discussed here suggest the following simulation to-do items:

– shaken-fluxtube Ca II H & K emission;

– cool-star Wilson-Bappu relation;

– umbral flashes and running penumbral waves;

– granular overshoot and gravity wave excitation;

– gravity wave interaction with fluxtubes and canopies;

– cool-star basal flux evaluation.

References

Alissandrakis, C. E., Georgakilas, A. A., & Dialetis, D. 1992, Sol. Phys., 138, 93

Athay, R. G. 1970, Sol. Phys., 11, 347

Ayres, T. R. 1979, ApJ, 228, 509

Ayres, T. R. 1981, ApJ, 244, 1064

Ayres, T. R. & Brault, J. W. 1990, ApJ, 363, 705

Ayres, T. R. & Rabin, D. 1996, ApJ, 460, 1042

Ayres, T. R. & Testerman, L. 1981, ApJ, 245, 1124

Ayres, T. R., Testerman, L., & Brault, J. W. 1986, ApJ, 304, 542

Ayres, T. R. & Wiedemann, G. R. 1989, ApJ, 338, 1033

Balthasar, H. 1999, Sol. Phys., 187, 389

Beckers, J. M. & Tallant, P. E. 1969, Sol. Phys., 7, 351

Bogdan, T. J., Rosenthal, C. S., Carlsson, M., et al. 2002, Astronomische Nachrichten, 323, 196

Bonet, J. A., Marquez, I., Vázquez, M., & Wöhl, H. 1991, A&A, 244, 492

Brandt, P. N., Rutten, R. J., Shine, R. A., & Trujillo Bueno, J. 1992, in Astronomical Society of the Pacific Conference Series, Vol. 26, Cool Stars, Stellar Systems, and the Sun, ed. M. S. Giampapa & J. A. Bookbinder, 161

Brandt, P. N., Rutten, R. J., Shine, R. A., & Trujillo Bueno, J. 1994, in Solar Surface Magnetism, ed. R. J. Rutten & C. J. Schrijver, 251

Braun, D. C. & Lindsey, C. 1999, ApJ, 513, L79

Braun, D. C., Lindsey, C., Fan, Y., & Jefferies, S. M. 1992, ApJ, 392, 739

Brisken, W. F. & Zirin, H. 1997, ApJ, 478, 814

Brown, T. M., Bogdan, T. J., Lites, B. W., & Thomas, J. H. 1992, ApJ, 394, L65

Brown, T. M. & Harrison, R. L. 1980, ApJ, 236, L169

Bruls, J. H. M. J., Rutten, R. J., & Shchukina, N. G. 1992, A&A, 265, 237

Brynildsen, N., Leifsen, T., Kjeldseth-Moe, O., Maltby, P., & Wilhelm, K. 1999, ApJ, 511, L121

Brynildsen, N., Maltby, P., Fredvik, T., & Kjeldseth-Moe, O. 2002, Sol. Phys., 207, 259

Bünte, M., Solanki, S. K., & Steiner, O. 1993, A&A, 268, 736

Cadez, V. M., Csik, A., Erdelyi, R., & Goossens, M. 1997, A&A, 326, 1241

Carlsson, M., Judge, P. G., & Wilhelm, K. 1997, ApJ, 486, L63

Carlsson, M. & Stein, R. F. 1994, in Chromospheric Dynamics, ed. M. Carlsson, 47

Carlsson, M. & Stein, R. F. 1995, ApJ, 440, L29

Carlsson, M. & Stein, R. F. 1996, in Astronomical Society of the Pacific Conference Series, Vol. 109, Cool Stars, Stellar Systems, and the Sun, ed. R. Pallavicini & A. K. Dupree, 119

Carlsson, M. & Stein, R. F. 1997, ApJ, 481, 500

Carlsson, M. & Stein, R. S. 1999, in Astronomical Society of the Pacific Conference Series, Vol. 184, Third Advances in Solar Physics Euroconference: Magnetic Fields and Oscillations, ed. B. Schmieder, A. Hofmann, & J. Staude, 206–210

Christopoulou, E. B., Georgakilas, A. A., & Koutchmy, S. 2000, A&A, 354, 305

Christopoulou, E. B., Georgakilas, A. A., & Koutchmy, S. 2001, A&A, 375, 617

Collados, M. 2002, Astronomische Nachrichten, 323, 254

Cram, L. E. 1972, Sol. Phys., 22, 375

Cram, L. E. 1978, A&A, 70, 345

Cram, L. E. & Damé, L. 1983, ApJ, 272, 355

Cuntz, M., Rammacher, W., Ulmschneider, P., Musielak, Z. E., & Saar, S. H. 1999, ApJ, 522, 1053

Curdt, W. & Heinzel, P. 1998, ApJ, 503, L95

Deubner, F. 1976, A&A, 51, 189

Deubner, F. 1991, in Mechanisms of Chromospheric and Coronal Heating, ed. P. Ulmschneider, E. R. Priest, & R. Rosner, 6

Deubner, F. 1998, in IAU Symposium, Vol. 185, New Eyes to See Inside the Sun and Stars, ed. F.-L. Deubner, J. Christensen-Dalsgaard, & D. Kurtz, 427

Deubner, F., Endler, F., & Staiger, J. 1984, Mem. Soc. Astron. Ital., 55, 135

Deubner, F. & Fleck, B. 1989, A&A, 213, 423

Deubner, F. & Fleck, B. 1990, A&A, 228, 506

Deubner, F., Fleck, B., Schmitz, F., & Straus, T. 1992, A&A, 266, 560

Deubner, F. & Gough, D. 1984, ARA&A, 22, 593

Deubner, F., Waldschik, T., & Steffens, S. 1996, A&A, 307, 936

Doyle, J. G., van den Oord, G. H. J., O'Shea, E., & Banerjee, D. 1998, Sol. Phys., 181, 51

Doyle, J. G., van den Oord, G. H. J., O'Shea, E., & Banerjee, D. 1999, A&A, 347, 335

Durrant, C. J. 1980, A&A, 91, 251

Durrant, C. J. & Nesis, A. 1981, A&A, 95, 221

Duvall, Jr., T. L. 1982, Nat, 300, 242

Duvall, Jr., T. L., Jefferies, S. M., Harvey, J. W., & Pomerantz, M. A. 1993, Nat, 362, 430

Emonet, T. & Cattaneo, F. 2001, ApJ, 560, L197

Endler, F. & Deubner, F. 1983, A&A, 121, 291

Erdélyi, R., Petrovay, K., Roberts, B., & Aschwanden, M. 2003, Turbulence, Waves and Instabilities in the Solar Plasma, ed. Erdélyi, R., Petrovay, K., Roberts, B., & Aschwanden, M.

Fawzy, D., Rammacher, W., Ulmschneider, P., Musielak, Z. E., & Stępień, K. 2002a, A&A, 386, 971

Fawzy, D., Stępień, K., Ulmschneider, P., Rammacher, W., & Musielak, Z. E. 2002b, A&A, 386, 994

Fawzy, D., Ulmschneider, P., Stępień, K., Musielak, Z. E., & Rammacher, W. 2002c, A&A, 386, 983

Fontenla, J. M., Avrett, E. H., & Loeser, R. 1993, ApJ, 406, 319

Frazier, E. N. 1968, ApJ, 152, 557

Gelfreikh, G. B., Grechnev, V., Kosugi, T., & Shibasaki, K. 1999, Sol. Phys., 185, 177

Georgakilas, A. A., Christopoulou, E. B., & Koutchmy, S. 2000, A&A, 363, 306

Georgakilas, A. A., Muglach, K., & Christopoulou, E. B. 2002, ApJ, 576, 561

Giovanelli, R. G. 1980, Sol. Phys., 68, 49

Giovanelli, R. G. & Jones, H. P. 1982, Sol. Phys., 79, 267

Gouttebroze, P., Vial, J., Bocchialini, K., Lemaire, P., & Leibacher, J. W. 1999, Sol. Phys., 184, 253

Hasan, S. S. & Kalkofen, W. 1999, ApJ, 519, 899

Hasan, S. S., Kalkofen, W., & van Ballegooijen, A. A. 2000, ApJ, 535, L67

Hindman, B. W. & Brown, T. M. 1998, ApJ, 504, 1029

Hoekzema, N. M., Rimmele, T. R., & Rutten, R. J. 2002, A&A, 390, 681

Hoekzema, N. M., Rimmele, T. R., & Rutten, R. J. 2002, A&A, 390, 681

Hoekzema, N. M. & Rutten, R. J. 1998, A&A, 329, 725

Hoekzema, N. M., Rutten, R. J., Brandt, P. N., & Shine, R. A. 1998, A&A, 329, 276

Hofmann, J., Steffens, S., & Deubner, F. 1996, A&A, 308, 192

Jones, H. P. & Giovanelli, R. G. 1982, Sol. Phys., 79, 247

Judge, P., Carlsson, M., & Wilhelm, K. 1997, ApJ, 490, L195

Judge, P. G., Tarbell, T. D., & Wilhelm, K. 2001, ApJ, 554, 424

Kalkofen, W. 2001, ApJ, 557, 376

Kalkofen, W., Ulmschneider, P., & Avrett, E. H. 1999, ApJ, 521, L141

Khomenko, E. V., Collados, M., & Bellot Rubio, L. R. 2003, ApJ, 588, 606

Kneer, F. 1983, A&A, 128, 311

Kneer, F. & von Uexküll, M. 1985, A&A, 144, 443

Kneer, F. & von Uexküll, M. 1986, A&A, 155, 178

Kneer, F. & von Uexküll, M. 1993, A&A, 274, 584

Komm, R., Mattig, W., & Nesis, A. 1991, A&A, 252, 827

Krijger, J. M. 2002, Structure and dynamics of the solar chromosphere (Utrecht University: PhD thesis)

Krijger, J. M., Rutten, R. J., Lites, B. W., et al. 2001, A&A, 379, 1052

Kumar, P. 1994, ApJ, 428, 827

Kupke, R., Labonte, B. J., & Mickey, D. L. 2000, Sol. Phys., 191, 97

Leibacher, J., Gouttebroze, P., & Stein, R. F. 1982, ApJ, 258, 393

Lin, H. & Rimmele, T. 1999, ApJ, 514, 448

Lindsey, C. & Braun, D. C. 1999, ApJ, 510, 494

Lites, B. 1994, in Chromospheric Dynamics, ed. M. Carlsson, 1

Lites, B. W. 1986, ApJ, 301, 1005

Lites, B. W. 1992, in NATO ASIC Proc. 375: Sunspots. Theory and Observations, ed. J. H. Thomas & N. O. Weiss, 261–302

Lites, B. W. & Chipman, E. G. 1979, ApJ, 231, 570

Lites, B. W., Rutten, R. J., & Berger, T. E. 1999, ApJ, 517, 1013

Lites, B. W., Rutten, R. J., & Kalkofen, W. 1993, ApJ, 414, 345

Lites, B. W., Rutten, R. J., & Thomas, J. H. 1994, in Solar Surface Magnetism, ed. R. J. Rutten & C. J. Schrijver, 159

Lites, B. W., Thomas, J. H., Bogdan, T. J., & Cally, P. S. 1998, ApJ, 497, 464

Liu, S. & Skumanich, A. 1974, Sol. Phys., 38, 109

Maltby, P., Brynildsen, N., Fredvik, T., Kjeldseth-Moe, O., & Wilhelm, K. 1999, Sol. Phys., 190, 437

Maltby, P., Brynildsen, N., Kjeldseth-Moe, O., & Wilhelm, K. 2001, A&A, 373, L1

McIntosh, S. W., Bogdan, T. J., Cally, P. S., et al. 2001, ApJ, 548, L237

McIntosh, S. W. & Judge, P. G. 2001, ApJ, 561, 420

Mein, N. & Schmieder, B. 1981, A&A, 97, 310

Mein, P., Mein, N., Malherbe, J. M., & Damé, L. 1987, A&A, 177, 283

Mihalas, B. W. & Toomre, J. 1981, ApJ, 249, 349

Mihalas, B. W. & Toomre, J. 1982, ApJ, 263, 386

Musielak, Z. E., Rosner, R., & Ulmschneider, P. 2002, ApJ, 573, 418

Musielak, Z. E. & Ulmschneider, P. 2002a, A&A, 386, 606

Musielak, Z. E. & Ulmschneider, P. 2002b, A&A, 386, 615

Nindos, A., Alissandrakis, C. E., Gelfreikh, G. B., Bogod, V. M., & Gontikakis, C. 2002, A&A, 386, 658

Nindos, A. & Zirin, H. 1998, Sol. Phys., 179, 253

Noyes, R. W. 1967, in IAU Symposium, Vol. 28, Aerodynamic Phenomena in Stellar Atmospheres, ed. R. N. Thomas, 293

Pintér, B., Erdélyi, R., & New, R. 2001, A&A, 372, L17

Rammacher, W. & Ulmschneider, P. 1992, A&A, 253, 586

Rosenthal, C. S., Bogdan, T. J., Carlsson, M., et al. 2002, ApJ, 564, 508

Rouppe van der Voort, L. H. M., Rutten, R. J., Sütterlin, P., Sloover, P. J., & Krijger, J. M. 2003, A&A, 403, 277

Rutten, R. J. 1995, in ESA Special Publication, Vol. 376, Helioseismology, 151

Rutten, R. J. 2001, in Astronomical Society of the Pacific Conference Series, Vol. 223, 11th Cambridge Workshop on Cool Stars, Stellar Systems and the Sun, ed. R. J. García López, R. Rebolo, & M. R. Zapaterio Osorio, 117

Rutten, R. J. & Krijger, J. M. 2003, A&A, 407, 735

Rutten, R. J. & Uitenbroek, H. 1991a, Sol. Phys., 134, 15

Rutten, R. J. & Uitenbroek, H. 1991b, in Mechanisms of Chromospheric and Coronal Heating, ed. P. Ulmschneider, E. R. Priest, & R. Rosner, 48

Schmieder, B. 1976, Sol. Phys., 47, 435

Schmieder, B. 1977, Sol. Phys., 54, 269

Schmieder, B. & Mein, N. 1980, A&A, 84, 99

Schrijver, C. J. 1995, A&AR, 6, 181

Schrijver, C. J. & Title, A. M. 2002, Sol. Phys., 207, 223

Schrijver, C. J., Title, A. M., Berger, T. E., et al. 1999, Sol. Phys., 187, 261

Settele, A., Sigwarth, M., & Muglach, K. 2002, A&A, 392, 1095

Shibasaki, K. 2001, ApJ, 550, 1113

Sivaraman, K. R., Gupta, S. S., Livingston, W. C., et al. 2000, A&A, 363, 279

Skartlien, R., Stein, R. F., & Nordlund, Å. 2000, ApJ, 541, 468

Socas-Navarro, H., Trujillo Bueno, J., & Ruiz Cobo, B. 2001, ApJ, 550, 1102

Staiger, J. 1987, A&A, 175, 263

Staiger, J., Mattig, W., Schmieder, B., & Deubner, F. 1984, Mem. Soc. Astron. Ital., 55, 147

Staude, J. 2002, Astronomische Nachrichten, 323, 317

Steffens, S., Deubner, F., Fleck, B., et al. 1997, in Astronomical Society of the Pacific Conference Series, Vol. 118, 1st Advances in Solar Physics Euroconference. Advances in Physics of Sunspots, ed. B. Schmieder, J. C. del Toro Iniesta, & M. Vázquez, 284

Steffens, S., Deubner, F., Hofmann, J., & Fleck, B. 1995, A&A, 302, 277

Stein, R. F. 1967, Sol. Phys., 2, 385

Stein, R. F. & Carlsson, M. 1997, in Astrophysics and Space Science Library, Vol. 225, SCORe'96 : Solar Convection and Oscillations and their Relationship, ed. F. P. Pijpers, J. Christensen-Dalsgaard, & C. S. Rosenthal, 261–276

Stein, R. F. & Nordlund, A. 1998, ApJ, 499, 914

Straus, T. & Bonaccini, D. 1997, A&A, 324, 704

Strous, L. H. 1994, PhD thesis, PhD Thesis, Utrecht University, (1994)

Sutmann, G. & Ulmschneider, P. 1995, A&A, 294, 241

Theurer, J., Ulmschneider, P., & Cuntz, M. 1997a, A&A, 324, 587

Theurer, J., Ulmschneider, P., & Kalkofen, W. 1997b, A&A, 324, 717

Thomas, J. H., Cram, L. E., & Nye, A. H. 1984, ApJ, 285, 368

Thomas, J. H. & Stanchfield, II, D. C. H. 2000, ApJ, 537, 1086

Thomas, R. N., ed. 1967, IAU Symposium, Vol. 28, Aerodynamic phenomena in stellar atmospheres, proceedings from Symposium no. 28 held at the Centre international d'astrophysique de l'observatoire de Nice, 2-14 September, 1965.

Toner, C. G. & Labonte, B. J. 1993, ApJ, 415, 847

Ulmschneider, P., Fawzy, D., Musielak, Z. E., & Stępień, K. 2001a, ApJ, 559, L167

Ulmschneider, P., Musielak, Z. E., & Fawzy, D. E. 2001b, A&A, 374, 662

Ulmschneider, P., Theurer, J., & Musielak, Z. E. 1996, A&A, 315, 212

Vernazza, J. E., Avrett, E. H., & Loeser, R. 1973, ApJ, 184, 605

Vernazza, J. E., Avrett, E. H., & Loeser, R. 1976, ApJS, 30, 1

Vernazza, J. E., Avrett, E. H., & Loeser, R. 1981, ApJS, 45, 635

von Uexküll, M., Kneer, F., Malherbe, J. M., & Mein, P. 1989, A&A, 208, 290

Whitaker, W. A. 1963, ApJ, 137, 914

Wikstøl, Ø., Hansteen, V. H., Carlsson, M., & Judge, P. G. 2000, ApJ, 531, 1150

Wilson, O. C. & Vainu Bappu, M. K. 1957, ApJ, 125, 661

Worden, J., Harvey, J., & Shine, R. 1999, ApJ, 523, 450

Zirin, H. & Stein, A. 1972, ApJ, 178, L85